

## OBSERVATIONAL UPPER BOUND ON THE COSMIC ABUNDANCES OF NEGATIVE-MASS COMPACT OBJECTS AND ELLIS WORMHOLES FROM THE SLOAN DIGITAL SKY SURVEY QUASAR LENS SEARCH

RYUICHI TAKAHASHI &amp; HIDEKI ASADA

Faculty of Science and Technology, Hirosaki University, Hirosaki 036-8561, Japan

*Draft version April 16, 2013*

## ABSTRACT

The latest result in the Sloan Digital Sky Survey Quasar Lens Search (SQLS) has set the first cosmological constraints on negative-mass compact objects and Ellis wormholes. There are no multiple images lensed by the above two exotic objects for  $\sim 50000$  distant quasars in the SQLS data. Therefore, an upper bound is put on the cosmic abundances of these lenses. The number density of negative mass compact objects is  $n < 10^{-8}(10^{-4})h^3\text{Mpc}^{-3}$  at the mass scale  $|M| > 10^{15}(10^{12})M_\odot$ , which corresponds to the cosmological density parameter  $|\Omega| < 10^{-4}$  at the galaxy and cluster mass range  $|M| = 10^{12-15}M_\odot$ . The number density of the Ellis wormhole is  $n < 10^{-4}h^3\text{Mpc}^{-3}$  for a range of the throat radius  $a = 10 - 10^4\text{pc}$ , which is much smaller than the Einstein ring radius.

*Subject headings:* gravitational lensing: strong – Cosmology: observations

## 1. INTRODUCTION

In theoretical physics, negative mass is a hypothetical concept of matter whose mass is of opposite sign to the mass of normal matter. Negative mass could thus generate the *repulsive* gravitational force. Although possible negative mass ideas have been often discussed since the 19th century, there has been no evidence for them (Bondi 1957; Jammer 1961, 1999). Even if its gravitational mass is negative, its inertial mass can be positive or negative (e.g. Jammer 1961). If the inertial mass is positive, the negative mass repels the ordinary matter (positive-mass objects) and hence it is likely to escape from the Milky Way. The negative masses attract each other to form a *negative* massive clump. Such clumps might reside in cosmological voids (e.g. Piran 1997). If the inertial mass is negative, on the other hand, the negative mass acts gravitationally as the ordinary matter. In this case, the negative masses could thus reside in the Galactic halo.

The gravitational lensing by the negative mass is the same as that by the positive mass, but its deflection angle has the opposite sign. Several authors have suggested that the negative masses could be detected in the Galactic microlensing (Cramer et al. 1995; Safonova et al. 2001a). Torres et al. (1998) assumed that the lensing of the distant active galactic nuclei by the hypothetical negative mass could be detected as the gamma ray burst and they provided the constraint on its mass density as  $|\rho| \lesssim 10^{-36}\text{gcm}^{-3}$  (corresponding to the cosmological density parameter  $|\Omega| \lesssim 10^{-7}$ ) around the mass scale of  $|M| \sim 0.1M_\odot$ .

The wormhole is a hypothetical object connecting distant regions of the universe, like a space-time tunnel. Ellis found a wormhole solution of the Einstein equation in general relativity by introducing a massless scalar field (Ellis 1973). Later, Morris & Thorne (1988) and Morris, Thorne & Yurtsever (1988) studied this solution as the traversable wormhole. The energy condition would be violated in order to create and maintain the wormhole (Visser 1995). Dark energy that could violate the energy condition is introduced to explain the observed accel-

ated expansion of the universe. The Ellis wormhole is massless and does not gravitationally interact with ordinary matter at remote distance. Hence, it makes no contribution to the cosmic mass density, even if it lives in our universe. However, it can deflect the light path. Recently, Abe (2010) has suggested that the wormhole at the throat radius of  $100 - 10^7\text{km}$  could be constrained (or detected) by using the Galactic microlensing. Although its abundance is quite unknown, some authors speculated that it is as abundant as stars in the universe (Krasnikov 2000; Abe 2010). More recently, Yoo et al. (2013) gave the rough upper bound of its number density as  $n \lesssim 10^{-9}\text{AU}^{-3}$  for the throat radius  $a \sim 1\text{cm}$  from the femtolensing of distant gamma ray bursts (Barnacka et al. 2012).

Although there are a lot of theoretical works concerning negative-mass objects and Ellis wormholes (e.g., Morris & Thorne 1988; Cramer et al. 1995; Visser 1995), observational studies have been very rare, mainly because no matter accretion occurs owing to the repulsive force by the negative mass and the Ellis wormhole, and it is thus unlikely to directly see them as luminous objects. Hence, it has recently attracted interests to study the gravitational lensing as an observational tool to probe such exotic dark objects (Kitamura et al. 2013; Tsukamoto & Harada 2013).

When a light ray from a distant quasar passes near the above lens objects (the negative mass and the Ellis wormhole), multiple images of the quasar are formed without any normal lens object. The absence of such multiple images can limit the cosmological abundances of these lens objects. The purpose of this letter is to place a first upper bound on the cosmic abundances of such exotic objects using the latest gravitational lensing survey. The SQLS has the current largest quasar lens sample from the SDSS II Data Release 7 (York et al. 2000). There are 50,836 quasars in the redshift range of  $z = 0.6 - 2.2$  with the apparent magnitude brighter than  $i = 19.1$ . The SQLS searched the lens systems in the image angular separation of  $1'' - 20''$  and found 19 lensed quasars (Oguri et al. 2006, 2008, 2012; Inada et

al. 2012). Note that this is currently the largest homogeneous sample for all the wavelengths of light. However, there is no lensed image candidate formed by unseen lens objects<sup>1</sup> such as the cosmic string, the black hole, and the dark halo (Oguri & Kayo, private communications). Hence, the absence of the unusual lensed quasar gives a strong constraint on the abundances of such exotic lens objects.

Throughout this paper, we employ the units of  $G = c = 1$  and use the cosmological parameters of the Hubble constant  $h = 0.7$ , the matter density  $\Omega_m = 0.28$  and the cosmological constant  $\Omega_\Lambda = 0.72$ , which is in concordance with the latest WMAP 9yr result (Hinshaw et al. 2012).

## 2. GRAVITATIONAL LENSING BY NEGATIVE-MASS COMPACT OBJECTS AND ELLIS WORMHOLES

### 2.1. Negative-mass compact object

The lensing by the negative-mass compact object could be described by the Schwarzschild lens with its negative mass  $M < 0$ . The lensing properties such as image positions and magnifications were theoretically studied by Cramer et al. (1995) and Safonova et al. (2001a,b). The image angular position  $\theta$  and the source position  $\beta$  are related via the lens equation,

$$\beta = \theta + \frac{\theta_E^2}{\theta}, \quad (1)$$

with the Einstein angular radius,

$$\theta_E = \left( 4 |M| \frac{D_{LS}}{D_L D_S} \right)^{1/2}, \quad (2)$$

where  $D_L$  and  $D_S$  are the angular-diameter distances to the lens and the source,  $D_{LS}$  is the distance from the lens to the source. The number of images depends on the source position: no image forms for  $\beta < 2\theta_E$ , one image forms for  $\beta = 2\theta_E$ , and the two images form for  $\beta > 2\theta_E$  at the positions  $\theta_{\pm} = (\beta \pm \sqrt{\beta^2 - 4\theta_E^2})/2$ . The image angular separation is  $\Delta\theta = |\theta_+ - \theta_-|$ . The magnification of each image is  $\mu_{\pm} = |1 - \theta_E^4/\theta_{\pm}^4|$ .

We obtain a relation between the typical lens mass and the image angular separation from Eq.(2) as,  $|M| \simeq 1 \times 10^{11} h^{-1} M_\odot (\theta_E/1'')^2 [(D_L D_S/D_{LS})/(1h^{-1} \text{Gpc})]$ . As a result, the sensitive mass range is  $|M| = 10^{11-14} M_\odot$  for the image separation of  $1'' - 20''$ .

### 2.2. Ellis wormhole lens

The Ellis wormhole is known to be a massless wormhole, which means that the asymptotic mass at infinity is zero. However, this wormhole deflects light by gravitational lensing (Clément 1984; Chetouani & Clément 1984; Perlick 2004; Nandi et al. 2006; Dey & Sen 2008; Nakajima & Asada 2012; Gibbons & Vyska 2012) because of its local curvature of the spacetime. The Ellis wormhole is characterized by one parameter as its throat radius  $a$ , and the line element is  $ds^2 = dt^2 - dr^2 - (r^2 +$

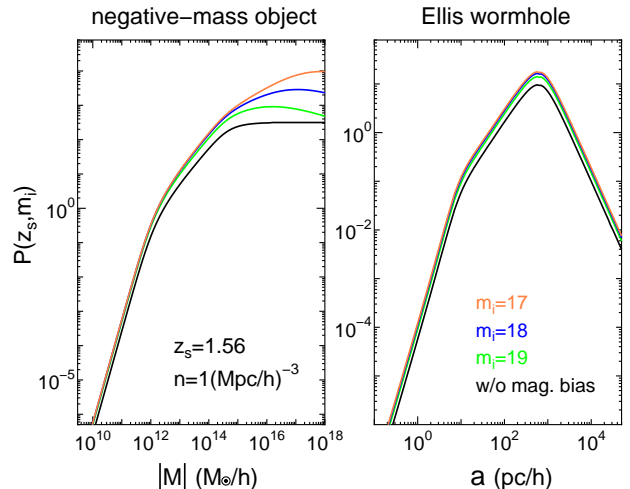


FIG. 1.— Multiple lensing probability that a quasar at the redshift  $z_s$  is lensed by a foreground lens object. Left: Negative-mass objects. Right: Ellis wormholes. The horizontal axis is the absolute value of mass  $|M|$  (left panel) and the throat radius  $a$  (right panel). The source redshift is set to be  $z_s = 1.56$  that is the mean redshift of statistical sample. We consider three cases for the apparent magnitude of the observed quasar as  $m_i = 17$  (orange curve), 18 (blue) and 19 (green). The black curve is the result without the magnification bias. Note that the probability is for the fixed number density of the lens  $n = 1h^3 \text{Mpc}^{-3}$  and the result scales as  $P \propto n$ .

$a^2)(d\theta^2 + \sin^2 \theta d\phi^2)$ . For Ellis wormholes, the lens equation in the weak field approximation becomes,

$$\beta = \theta - \theta_E^3 \frac{\theta}{|\theta|^3}, \quad (3)$$

with the Einstein angular radius,

$$\theta_E = \left( \frac{\pi a^2}{4} \frac{D_{LS}}{D_L^2 D_S} \right)^{1/3}. \quad (4)$$

The two images form irrespective of the source position at the angular positions,  $x_{\pm}^{-1} = \pm \sqrt[3]{1/2 + \sqrt{1/4 \pm y^3/27}} - \sqrt[3]{\mp 1/2 \pm \sqrt{1/4 \pm y^3/27}}$ , where  $x_{\pm} = \theta_{\pm}/\theta_E$  and  $y = \beta/\theta_E$  (Toki et al. 2011; Nakajima & Asada 2012). The magnification for each image is  $\mu_{\pm} = |(1 \mp x_{\pm}^{-3})(2x_{\pm}^{-3} \pm 1)|^{-1}$ .

The typical throat radius for a given  $\theta_E$  is estimated as,  $a \simeq 10 h^{-1} \text{pc} (\theta_E/1'')^{3/2} [(D_L^2 D_S/D_{LS})/(1h^{-1} \text{Gpc})^2]^{1/2}$ , from Eq.(4). As a result, the sensitive throat radius is  $a = 10 - 100 \text{pc}$  from the image separation of  $1'' - 20''$ . Note that the relevant throat radius is much smaller than the corresponding Einstein ring radius  $R_E = \theta_E \times D_L \sim 10 \text{kpc} (\theta_E/1'') (D_L/1h^{-1} \text{Gpc})$ . In practice, the range of the radius is slightly wider, since the lensing effects are dependent also on the distance ratios.

## 3. STRONG LENSING PROBABILITY

In this section, we discuss the lensing probability that a distant quasar is lensed by the foreground negative-mass object or the Ellis wormhole. We assume that the lens objects are uniformly distributed in the Universe. We basically follow the calculation in the SQLS (Oguri et al. 2012). The basics of the lensing probability is discussed in Schneider et al. (1992, 2006). The probability is roughly estimated as a product of the distance

<sup>1</sup> This paper assumes that the negative masses are unseen. However, they might form stars (or galaxies) to emit radiation like the usual matter. In this case, it would be difficult to distinguish the negative mass object from the positive one if these spectral energy distributions are the same. However the spectra of such negative-mass stars are quite unknown.

to the quasar  $D_S$ , the number density of the lens  $n$ , and the cross section  $\sigma$ , i.e.  $P \sim n\sigma D_S$ . Here, the cross section is defined in the lens plane and is roughly given by  $\sigma \sim \pi(D_L\theta_E)^2$ .

First, we evaluate the cross section. The SQLS searched multiple quasar images with the image separation range of  $1'' < \Delta\theta < 20''$  and with the flux ratio  $\mu_+/\mu_-$  less than  $10^{-0.5}$ . Then, the cross section to form multiple images is

$$\sigma = 2\pi D_L^2 \int_{\beta_{\min}}^{\beta_{\max}} d\beta \frac{\Phi(L/\mu, z_s)}{\mu\Phi(L, z_s)} \Theta\left(10^{-0.5} - \frac{\mu_+}{\mu_-}\right) \times \Theta(\Delta\theta - 1'')\Theta(20'' - \Delta\theta) \quad (5)$$

where  $\Theta(x)$  is the step function:  $\Theta(x) = 1$  for  $x \geq 0$  and  $\Theta(x) = 0$  for  $x < 0$ .  $\beta_{\min}$  and  $\beta_{\max}$  are the minimum and maximum source positions to form the multiple images:  $(\beta_{\min}, \beta_{\max}) = (2\theta_E, \infty)$ , and  $(0, \infty)$  for the negative-mass lens and the Ellis wormhole. Note that the image separation  $\Delta\theta$  and the flux ratio  $\mu_+/\mu_-$  in the integrand of Eq.(5) are a function of  $\beta$ .  $\Phi(L, z_s)$  is the quasar luminosity function at  $z_s$  and this term is so called the magnification bias which is a correction term for flux-limited survey. We use the same luminosity function as that used in Oguri et al. (2012) (see e.g. Croom et al. 2009; Richards et al. 2006).

We assume that the number density of the lens is constant in comoving scale. Then the lensing probability for the quasar at  $z_s$  with an apparent magnitude  $m_i$  is

$$P(z_s, m_i) = \int_0^{z_s} dz_l \frac{cdt}{dz_l} n (1+z_l)^3 \sigma \quad (6)$$

where  $z_l$  is the lens redshift and  $cdt/dz_l = 1/(H(z_l)(1+z_l))$  with the Hubble expansion rate  $H(z_l)$ .

Fig.1 shows the lensing probability for the quasar at the redshift  $z_s$  with the magnitude  $m_i$ . The source redshift is set to be  $z_s = 1.56$  which is the mean redshift of the statistical sample of quasars in the SQLS. The left panel is for the negative-mass compact object, and the right panel is for the Ellis wormhole. The horizontal axis is the absolute value of the lens mass  $|M|$  (left panel) and the throat radius  $a$  (right panel). The quasar magnitudes are  $m_i = 17$  (orange), 18 (blue) and 19 (green), and the black curve is the result without the magnification bias. The result is plotted for the fixed number density of the lens  $n = 1h^3\text{Mpc}^{-3}$  and the probability scales as  $P \propto n$ .

In order to evaluate the observational upper bound on the number density  $n$  of the lenses, we use the likelihood function introduced in Kochanek (1993),  $\ln L \simeq -\sum_{j=1}^{N_Q} P(z_{s,j}, m_{i,j})$ , where  $z_{s,j}$  and  $m_{i,j}$  are the redshift and the apparent magnitude of the  $j$ -th quasar.  $N_Q$  is the total number of statistical samples of quasars,  $N_Q = 50836$ . The data of  $z_{s,j}$  and  $m_{i,j}$  were downloaded from the SQLS website<sup>2</sup>.

#### 4. RESULTS

Fig.2 shows the upper bound on the cosmological number density of the negative-mass compact objects. The vertical axis is the number density  $n$  ( $h^3\text{Mpc}^{-3}$ ), while the horizontal axis is the absolute value of the mass  $|M|$  ( $h^{-1}M_\odot$ ). The two curves are the upper bound at

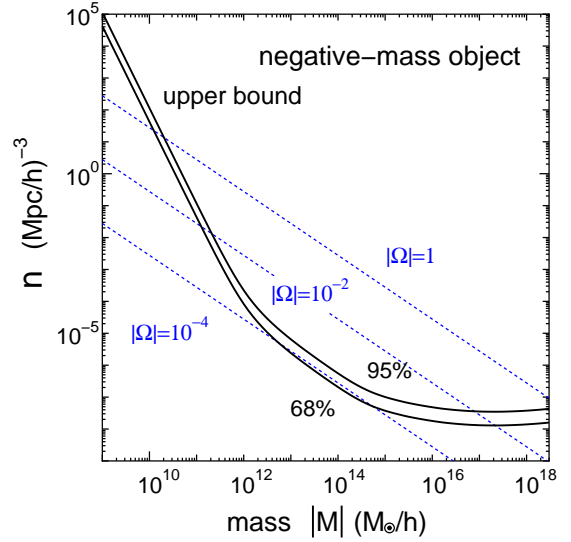


FIG. 2.— Upper bound on the cosmological number density of negative-mass compact objects. The vertical axis denotes the density  $n$  ( $h^3\text{Mpc}^{-3}$ ). The horizontal axis denotes the absolute value of the mass  $|M|$  ( $h^{-1}M_\odot$ ). The two solid curves correspond to upper bounds of 68% and 95% confidence levels. The blue dashed lines denote the absolute value of the cosmological density parameter for the negative mass,  $|\Omega| = 10^{-4}, 10^{-2}$  and 1.

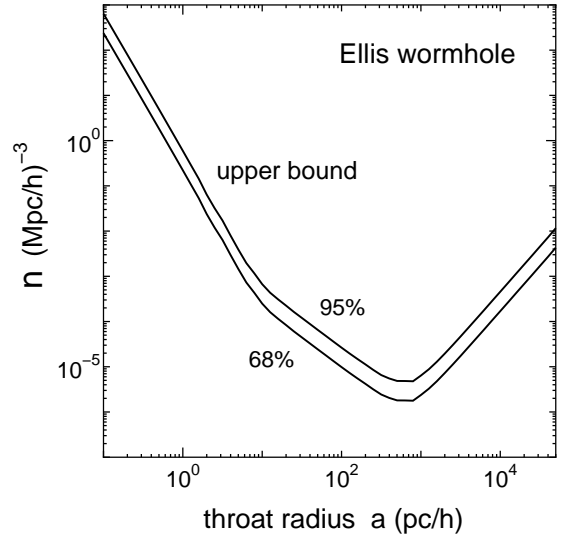


FIG. 3.— Same as Fig.2, but for the Ellis wormhole. The horizontal axis is the throat radius  $a$  ( $h^{-1}\text{pc}$ ).

68% and 95% confidence levels. It turns out that the number density is less than  $n < 10^{-7}(10^{-5})h^3\text{Mpc}^{-3}$  for  $|M| > 10^{14}(10^{12})M_\odot$ . The blue dashed lines show the absolute value of the cosmological density parameter,  $|\Omega| = 10^{-4}, 10^{-2}$  and 1. The density parameter is defined as the mass density divided by the cosmological critical density,  $\Omega = Mn/\rho_{\text{cr}}$ . As shown in the figure, the density parameter is less than  $|\Omega| < 10^{-4}$  for galactic and cluster mass scale  $|M| = 10^{12} - 10^{15}M_\odot$ . As a result, the negative-mass compact object is less abundant than the galaxy with typical luminosity  $L^*$  ( $n_{\text{gal}} \approx 10^{-2}\text{Mpc}^{-3}$ ) and the galaxy cluster with typical mass  $10^{14}M_\odot$  ( $n_{\text{clust}} \approx 10^{-4}\text{Mpc}^{-3}$ ), which correspond

<sup>2</sup> <http://www-utap.phys.s.u-tokyo.ac.jp/~sdss/sqls/>

to  $\Omega_{\text{gal}} \approx 0.2$  for the galaxies and  $\Omega_{\text{clust}} \approx 0.3$  for the clusters (e.g. Fukugita & Peebles 2004)

Fig.3 shows the Ellis wormhole cases. The horizontal axis is the throat radius  $a$  ( $h^{-1}\text{pc}$ ). As shown in the figure, the number density is  $n < 10^{-4}h^3\text{Mpc}^{-3}$  for  $a = 10 - 10^4\text{pc}$ . As a result, the Ellis wormhole with  $a = 0.1 - 10^5\text{pc}$  is much less abundant than a star ( $n_{\text{star}} \approx 10^{10}\text{Mpc}^{-3}$ ). Note that our extragalactic constraint is complementary to the galactic one by the microlensing that is sensitive for the smaller radius  $a = 100 - 10^7\text{km}$  (Abe 2010). The upper-bound curves in Fig.3 approach straight lines for very small  $a (\ll 0.1\text{pc})$  or large  $a (\gg 10^4\text{pc})$ . In the case of a very small  $a$ , the lens is very close to us since  $a \propto D_L$  from Eq.(4) under the fixed  $\theta_E$  and  $D_S$ , while the lens for a very large  $a$  is very close to the source since  $a \propto D_{LS}^{-1/2}$  from Eq.(4).

## 5. DISCUSSION AND CONCLUSION

We presented the upper bound on the cosmic abundances of the negative-mass compact object and the Ellis wormhole using the quasar lens sample in the SQLS data based on SDSS II. Our main results are summarized in Figs.2 and 3. On-going or future surveys such as Pan-Starrs<sup>3</sup>, Dark Energy Survey<sup>4</sup>, Subaru Hyper Suprime-Cam (Miyazaki et al. 2006), Large Synoptic Survey Telescope (LSST)<sup>5</sup> will find much more lensed quasars by the foreground galaxies than the SDSS II (Oguri & Marshall 2010). Especially, the LSST will find about 8000 lensed quasars which are much more than the 19 lensed quasars in the SQLS. Therefore, the LSST will provide over 100 times stronger constraint than the current upper bound shown in Figs.2 and 3, or might lead to a first detection

of such exotic lenses.

Note that our constraint for the negative masses can be applied only for the compact objects (i.e. its size is smaller than the Einstein radius). As mentioned in the introduction, the negative masses can attract each other to form a massive clump. For such negative-mass clouds, our upper bound in Fig.2 becomes weaker. For instance, one can show that the singular isothermal sphere lens composed of the negative masses does not form multiple images. In this case, the weak lensing is a more powerful tool to identify the negative-mass clumps. The negative masses could act as voids in the universe, since the void is the underdense region compared with the cosmic mean density and hence its convergence is *negative*. Several authors reported possible detections of voids by the weak lensing of background galaxies (e.g. Miyazaki et al. 2002; Gavazzi & Soucail 2007; Shan et al. 2012) and by the integrated Sachs-Wolfe effect in the Cosmic Microwave Background (e.g. Granett et al. 2008; Ilić et al. 2013; Cai et al. 2013). If the density contrast of the void were less than  $-1$ , it could be an evidence for the negative masses. Because of the low signal-to-noise ratio in the present analyses, the next generation surveys are awaited.

RT thanks Masamune Oguri and Issha Kayo for useful comments about the SQLS. HA would like to thank Fumio Abe, Matthias Bartelmann, Matt Visser, Koji Izumi, Takao Kitamura, and Koki Nakajima for stimulating conversations on the exotic lens models. RT is supported by Grant-in-Aid for Japan Society for the Promotion of Science (No. 25287062).

<sup>3</sup> <http://pan-starrs.ifa.hawaii.edu/public/>

<sup>4</sup> <http://www.darkenergysurvey.org/>

<sup>5</sup> <http://www.lsst.org/lsst/>

## REFERENCES

- Abe, F. 2010, ApJ, 725, 787  
 Barnacka, A., Glicenstein, J.-F., & Moderski, R. 2012, PRD, 86, 043001  
 Bondi, H. 1957, Rev. Mod. Phys., 29, 423  
 Cai, Y.-C., et al. 2013, submitted to ApJ, arXiv:1301.6136  
 Chetouani, L. & Clément, G. 1984, Gen. Relativ. Gravit. 16, 111  
 Clément, G. 1984, J. Theor. Phys. 23, 335  
 Croom, S.M., Richards, G.T., Shanks, T., et al., 2009, MNRAS, 399, 1755  
 Cramer, J. G., Forward, R. L., Morris, M. S., Visser, M., Benford, G., & Landis, G. A. 1995, Phys. Rev. D, 51, 3117  
 Dey, T. K. & Sen, S. 2008, Mod. Phys. Lett. A 23, 953  
 Ellis, H. G. 1973, J. Math. Phys., 14, 104  
 Fukugita, M. & Peebles, P.J.E. 2004, ApJ, 616, 643  
 Gavazzi, R. & Soucail, G. 2007, A&A, 462, 459  
 Gibbons, G. W., Vyska, M. 2012, Class. Quant. Grav. 29, 065016  
 Granett, B.R., Neyrinck, M.C., & Szapudi, I. 2008, ApJL, 683, L99  
 Hinshaw, G., Larson, D., Komatsu, E., et al., 2012, arXiv:1212.5226, submitted to ApJ Suppl.  
 Ilić, S., Langer, M. & Douspis, M. 2013, arXiv:1301.5849, submitted to A&A  
 Inada, N., Oguri, M., Shin, M.-S., et al., 2012, AJ, 143, 119  
 Jammer, M. 1961, Concepts of Mass in Classical and Modern Physics, (Cambridge, Harvard University Press)  
 Jammer, M. 1999, Concepts of Mass in Contemporary Physics and Philosophy, (Princeton, Princeton University Press)  
 Kitamura, T., Nakajima, K., Asada, H. 2013, Phys. Rev. D, 87, 027501  
 Kochanek, C.S., 1993, ApJ, 419, 12  
 Krasnikov, S. 2000, Phys. Rev. D, 62, 084028  
 Miyazaki, S., Hamana, T., Shimasaku, K., Furusawa, H., et al. 2002, ApJL, 580, L97  
 Miyazaki, S., Komiya, Y., & Nakaya, H. et al. 2006, Proc. SPIE, 6269, 9  
 Morris, M. S., & Thorne, K. S. 1988, Am. J. Ph., 56, 395  
 Morris, M.S., Thorne, K.S., & Yurtsever, U. 1988, Phys. Rev. Lett., 61, 1446  
 Nakajima, K. & Asada, H. 2012, Phys. Rev. D, 85, 107501  
 Nandi, K. K., Zhang, Y.-Z., & Zakharov, A. V. 2006, Phys. Rev. D, 74, 024020  
 Oguri, M., Inada, N., Pindor, B. et al., 2006, AJ, 132, 999  
 Oguri, M., Inada, N., Strauss, M.A. et al., 2008, AJ, 135, 512  
 Oguri, M. & Marshall, P.J., 2010, MNRAS, 405, 2579  
 Oguri, M., Inada, N., Strauss, M.A. et al., 2012, AJ, 143, 120  
 Perlick, V. 2004, Phys. Rev. D, 69, 064017  
 Piran, T. 1997, GRG, 29, 1363  
 Richards, G.T., Strauss, M.A., Fan, X., et al. 2006, AJ, 131, 2766  
 Safonova, M., Torres D.F., & Romero, G. E. 2001a, Phys. Rev. D, 65, 023001  
 Safonova, M., Torres D.F., & Romero, G. E. 2001b, Mod. Phys. Lett. A, 16, 153  
 Schneider, P., Ehlers, J., & Falco, E. E., 1992, Gravitational Lenses (Berlin: Springer)  
 Schneider, P., Kochanek, C., & Wambsganss, J., 2006, Gravitational Lensing: Strong, Weak and Micro (Berlin: Springer)  
 Shan, H.Y., Kneib, J.-P., Tao, C., Fan, Z., et al. 2012, ApJ, 748, 56  
 Toki, Y., Kitamura, T., Asada, H., & Abe, F., 2011, ApJ, 740, 121  
 Torres, D. F., Romero, G. E., & Anchordoqui, L. A. 1998, Phys. Rev. D, 58, 123001

- Tsukamoto, N., Harada, T. 2013, Phys. Rev. D, 87, 024024  
York et al. 2000, AJ, 120, 1579  
Visser, M. 1995, Lorentzian Wormholes: From Einstein to  
Hawking, (NY: AIP)  
Yoo, C.-M., Harada, T. & Tsukamoto, N. 2013, arXiv:1302.7170